Journal of Magnetism and Magnetic Materials 58 (1986) 128–134
North-Holland, Amsterdam

# $Mn_3O_4$ COMMENSURATE AND INCOMMENSURATE MAGNETIC STRUCTURES

B. CHARDON and F. VIGNERON

*Laboratoire Léon Brillouin (Laboratoire commun CEA-CNRS), CEN-Saclay, 91191 Gif-sur-Yvette Cedex, France*

Received 30 May 1985

The compound $Mn_3O_4$ (Hausmannite) was investigated by means of neutron diffraction in the temperature range between 4.2 K and $T_C = 43$ K, in order to study the commensurate–incommensurate magnetic transition at $T_t = 33$ K. Below $T_t$, the commensurate ferrimagnetic structure of $Mn_3O_4$ is known. Between $T_t$ and $T_C$, the incommensurate part of the magnetic structure of $Mn_3O_4$ is found to be sinusoidal, contrary to previous results (helimagnetic solution). The continuity of the magnetic structure at $T_t$, which is suggested by specific heat measurements, is now confirmed. The thermal variation of the propagation vector $\boldsymbol{\tau}//\boldsymbol{b}^*$ for the $Mn_3O_4$ magnetic structure has been obtained below $T_C$.

## 1. Introduction

### 1.1. Crystalline structure

$Mn_3O_4$ has a tetragonally distorted spinel structure, with space group $I4_1/amd$. At room temperature, the lattice parameters are $a = b = 5.763$ Å [1] and $c = 9.456$ Å [1], so that $c/a\sqrt{2} = 1.16$. $Mn_3O_4$ is a normal spinel [2]: the divalent and trivalent manganese ions occupy respectively the tetrahedral (A) and octahedral (B) sites of the spinel structure $AB_2O_4$. Table 1 gives the values of the crystallographic parameters for $Mn^{2+}$ and $Mn^{3+}$ ions in the crystalline unit cell of $I4_1/amd$: the atoms are labelled from 1 to 12 and separated into tetrahedral (T) and octahedral (R and S) sites.

Table 1
Crystallographic positions of $Mn^{2+}$ (A) and $Mn^{3+}$ (B) ions in the $I4_1/amd$ unit cell. $Mn^{2+}$ ions occupy sites 4 a and $Mn^{3+}$ are in sites 8 d. Atoms with a label $i$ going from 1 to 6 are indicated below; $i+6$ and $i'(1 < i' < 12)$ are deduced from $i$ after $[\frac{1}{2}, \frac{1}{2}, \frac{1}{2}]$ and [0, 1, 0] translations respectively

| | | $x$ | $y$ | $z$ |
|---|---|---|---|---|
| $Mn^{2+}$ | $T_1$ | 0 | 0 | 0 |
| | $T_2$ | 0 | $\frac{1}{2}$ | $\frac{1}{4}$ |
| | $R_3$ | 0 | $\frac{1}{4}$ | $\frac{5}{8}$ |
| $Mn^{3+}$ | $R_4$ | 0 | $\frac{3}{4}$ | $\frac{5}{8}$ |
| | $S_5$ | $\frac{1}{4}$ | 0 | $\frac{3}{8}$ |
| | $S_6$ | $\frac{3}{4}$ | 0 | $\frac{3}{8}$ |

### 1.2. Magnetic properties

Magnetic measurements indicate a ferrimagnetic behaviour for $Mn_3O_4$ [3,4], with a Curie temperature $T_C = 42$ K. The spontaneous magnetization below $T_C$ is directed along one of the main crystallographic axes in the (001) plane ($\boldsymbol{b}$ by convention). The $T = 0$ K extrapolated value of the resultant magnetization is $1.84\mu_B$ per $Mn_3O_4$, less than $3\mu_B$, as calculated in a collinear model of ferrimagnetism. The asymptotic Curie temperature is $T_a = -640$ K [4]. S. Srinivasan et al. [5] have analyzed the magnetic response of $Mn_3O_4$ in the framework of the Lotgering [6] formalism: the exchange constants $J_{AA}$, $J_{AB}$ and $J_{BB}$ are all antiferromagnetic, with predominant B–B interactions. The anomaly observed at $T = 39$ K in the $M$ versus $T$ data [5] is suggested to correspond to a transition from a non-collinear ($T < 39$ K) to a collinear (39 K < $T$ < 42 K) magnetic structure for $Mn_3O_4$.

### 1.3. Neutron diffraction data

From neutron diffraction data at $T = 4.2$ K, the commensurate magnetic structure of $Mn_3O_4$ has

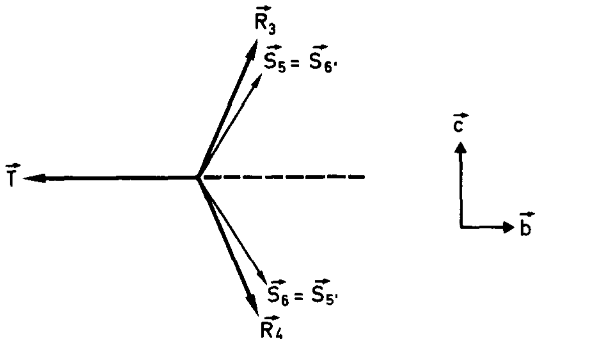


Fig. 1. The commensurate $a, 2a, c$ magnetic structure of $Mn_3O_4$ at $T < T_t = 33$K: $\boldsymbol{T} = \boldsymbol{T}_1 = \boldsymbol{T}_2$; $\boldsymbol{T}_{i+6} = \boldsymbol{T}_i$; $\boldsymbol{T}_{i'} = \boldsymbol{T}_i$; $\boldsymbol{R}_{i+6} = \boldsymbol{R}_i$; $\boldsymbol{R}_{i'} = \boldsymbol{R}_i$; $\boldsymbol{S}_{i+6} = \boldsymbol{S}_i$.

been obtained [1,7]. The magnetic cell is $a$, $2a$, $c$. The magnetic structure is depicted in fig. 1 and described as follows:

$Mn^{2+}$ magnetic moments: $\boldsymbol{T}_1 = \boldsymbol{T}_2$; $\boldsymbol{T}_{i+6} = \boldsymbol{T}_i$; $\boldsymbol{T}_{i'} = \boldsymbol{T}_i$ directed along the $\boldsymbol{b}$-axis, antiparallel to the resultant magnetic moment of the $Mn^{3+}$ ions.

$Mn^{3+}$ magnetic moments: $R$ and $S$ are to be distinguished. The magnetic arrangement is defined by $\boldsymbol{R}_3$, $\boldsymbol{R}_4$, $\boldsymbol{S}_5$ and $\boldsymbol{S}_6$ and $\boldsymbol{R}_{i+6} = \boldsymbol{R}_i$; $\boldsymbol{R}_{i'} = \boldsymbol{R}_i$; $\boldsymbol{S}_{i+6} = \boldsymbol{S}_i$ but $\boldsymbol{S}_{i'} \neq \boldsymbol{S}_i$ (cf. fig. 1). $\boldsymbol{R}_3$ and $\boldsymbol{R}_4$, $\boldsymbol{S}_5$ and $\boldsymbol{S}_6$ are lying in the ($\boldsymbol{b}$, $\boldsymbol{c}$) plane, in a symmetric way relative to the $\boldsymbol{b}$-axis, with slightly different values for $\theta_R = (\boldsymbol{b}, \boldsymbol{R})$ and $\theta_S = (\boldsymbol{b}, \boldsymbol{S})$ angles. $S_z$ is the only magnetic component leading to a doubled magnetic unit cell ($a$, $2a$, $c$).

Small deviations from this basic model are proposed: B. Boucher et al. [1] introduce $T_z$ and $S_x$ components (powder neutron diffraction study), G.B. Jensen et al. [7] introduce $R_x$ components (single-crystal study). These components do not modify the selection rules for the magnetic Bragg peaks; they only induce small changes in the magnetic intensities and will not be taken into account in our neutron diffraction study.

At $T_t = 33$ K a magnetic phase transition occurs for the cell doubling spin system ($S$). From the angular shift of the magnetic Bragg peaks, the propagation vector $\boldsymbol{\tau}$ varies then from $\boldsymbol{\tau} = \frac{1}{2}\boldsymbol{b}^*$ below $T_t$ to $\boldsymbol{\tau} = 0.47\boldsymbol{b}^*$ immediatly above $T_t$ [7]. The magnetic structure of the $Mn^{3+}$ S atoms is then conical [8], defined by:

$$S_{ix} = S\cos(2\pi\boldsymbol{\tau}\cdot\boldsymbol{r}_i + \varphi_0^i)$$

$$S_{iy} = S_{\parallel}$$

$$S_{iz} = S\sin(2\pi\boldsymbol{\tau}\cdot\boldsymbol{r}_i + \varphi_0^i)$$

and the subsequent relations between the initial phases $\varphi_0^i$:

$$\varphi_0^5 = \varphi_0^{11}; \qquad \varphi_0^6 = \varphi_0^{12}; \qquad \varphi_0^5 - \varphi_0^6 = \pi.$$

Let us notice that these two solutions ($T < T_t$ and $T > T_t$) for the magnetic structure of $Mn^{3+}$ atoms on S sites are not continuously deduced from each other at $T = T_t$. The situation is illustrated in fig. 2: (i) corresponds to the commensurate $a$, $2a$, $c$ magnetic structure below $T_t$ and (ii) to the helimagnetic part ($\boldsymbol{S}_\perp$) of the conical structure observed above $T_t$ and represented here in the case where $\boldsymbol{\tau} = \frac{1}{2}\boldsymbol{b}^*$. Yet this discontinuity has not been observed for $Mn_3O_4$ in specific heat measurements [8,9]. We have so reinvestigated $Mn_3O_4$ by means of neutron diffraction, in

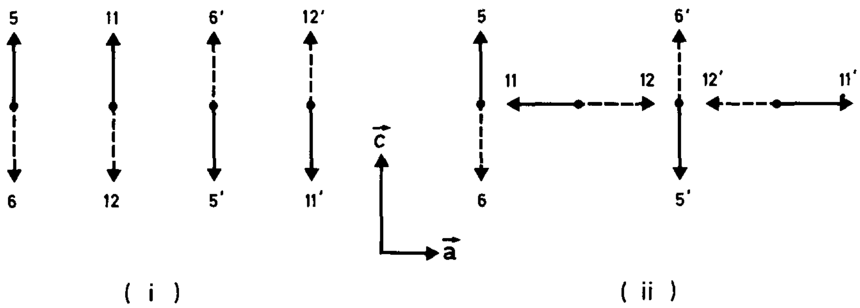


Fig. 2. Discontinuity of the $Mn_3O_4$ magnetic surstructure at $T_t = 33$ K. The $Mn^{3+}$ magnetic moments (S atoms: $S_x$ and $S_z$ components) are represented in a succession taking into account the $y$ coordinate only (cf. table 1). (i) $a, 2a, c$ commensurate magnetic structure below $T_t$; (ii) helimagnetic structure with a propagation vector $\boldsymbol{\tau} = \frac{1}{2}\boldsymbol{b}^*$.

order to study the commensurate–incommensurate magnetic transition at $T_t = 33$ K.

## 2. Experimental

A polycrystalline sample of $Mn_3O_4$ has been obtained [10] from a manganese oxide $MnO_x$, with $x \sim 1.8$, heated in air for 7 days at 1100°C and some hours at 1250°C.

The neutron diffraction experiments have been mainly performed at the Siloe Reactor in Grenoble (CEN-G), on a two-axis spectrometer ($\lambda = 2.5$ Å) with a Position Sensitive Detector (800 cells over $2\theta = 80°$) [11]. Some complementary results have been obtained at the Orphée Reactor in Saclay (CEN-S), on a classical two-axis spectrometer (Pyrrhias, $\lambda = 2.46$ Å).

The Rietveld profile analysis [12] has been used in a modified version, taking into account an incommensurate part for the magnetic structure. The possibility of simultaneous refinements for commensurate and incommensurate magnetic structure has only been introduced for the case of the isomorphous compounds $Mn_3O_4$ and $Zn_xMn_{3-x}O_4$.

## 3. $Mn_3O_4$ commensurate magnetic structure

### 3.1. $T = 4.2$ K

Neutron diffraction data at $T = 4.2$ K on polycrystalline $Mn_3O_4$ have been analyzed, using the Rietveld profile refinement technique [12], with the assumption of the non-collinear magnetic structure described in section 1.3 and fig. 1 (magnetic cell $a$, $2a$, $c$).

With $\lambda = 2.5$ Å and $2\theta$ running from 20 to 90°, the refined value for the magnetic moments $\boldsymbol{T}$, $\boldsymbol{R}_3$ and $\boldsymbol{S}_5$ are:

$T_y = -4.57(15)\mu_B$

$R_y = 1.38(16)\mu_B$

$R_z = 3.23(11)\mu_B$

$S_y = 1.30(20)\mu_B$

$S_z = 2.85(10)\mu_B$

with reliability factors [12] $R_N = 0.8$ and $R_M = 2.6$ (N = nuclear, M = magnetic).

From the above values, the resultant magnetic moment per $Mn_3O_4$ can be deduced: $1.89(50)\mu_B$. This result is in good agreement with the result ($1.84\mu_B$) of O.V. Nielsen [4], which has been obtained from magnetization measurements.

The oxygen positional parameters (16 h site) have been obtained at $T = 4.2$ K: $x = 0.2225$ (20) and $x = 0.3844$ (12).

### 3.2. Thermal variation of the $Mn_3O_4$ commensurate magnetic structure

The commensurate $a$, $2a$, $c$ magnetic structure is obtained for $Mn_3O_4$ up to $T_t = 33$ K, where a sudden shift is observed for the angular positions of the Bragg peaks associated with the cell doubling spin system (S atoms, $S_z$ components).

We report in fig. 3 the thermal variation of $T_y$, $R_y$ and $R_z$, $S_y$ and $S_z$ magnetic components below $T_t$. The thermal variation of the magnetic

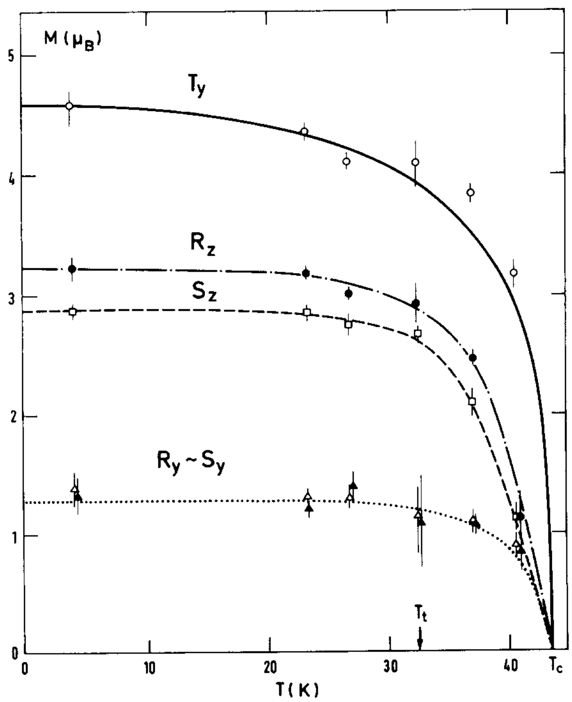


Fig. 3. Thermal variation of the $Mn_3O_4$ commensurate magnetic structure: $T_y$, $R_y$ and $R_z$, $S_y$ and $S_z$ components of the magnetic moments $\boldsymbol{T}$, $\boldsymbol{R}_3$ and $\boldsymbol{S}_5$ (see table 1 and fig. 1).

structure of $Mn_3O_4$ in the temperature range between $T_t$ and $T_C$ is studied in the next section.

## 4. $Mn_3O_4$ magnetic structure for $T_t < T < T_C$

### 4.1. $T = 37$ K

Neutron diffraction data on $Mn_3O_4$ in the temperature range between $T_t$ and $T_C$ are reported in fig. 4 ($T = 37$ K data measured on the two-axis spectrometer at Siloe, with $\lambda = 2.5$ Å). Two types of magnetic Bragg peaks are obtained, all indexed in the $a$, $a$, $c$ quadratic crystalline unit cell: $hkl_M$ and $hkl^{\pm}$.

$hkl_M$ Bragg peaks (selection rule: $h + k + l$ even) correspond to the magnetic components $T_y$, $R_y$, $R_z$ and $S_y$, as described in the commensurate structure in fig. 1.

$hkl^{\pm}$ Bragg peaks are observed only for reciprocal lattice points $\boldsymbol{G} = h\boldsymbol{a}^* + k\boldsymbol{b}^* + l\boldsymbol{c}^*$ with $h + k + l$ even and $h$ odd. The propagation vector $\boldsymbol{\tau}$, as deduced from the angular positions of the satellites $\boldsymbol{K} = \boldsymbol{G} \pm \boldsymbol{\tau}$, is equal to $0.44\boldsymbol{b}^*$ at $T = 37$ K. The incommensurate part of the magnetic structure of $Mn_3O_4$ is obtained from the intensity analysis of these satellites. Two types of solutions have been tried: a helimagnetic structure, as described in section 1.3 ($S_x$ and $S_z$ magnetic components) and a sinusoidal modulation [$S_z$ component only: $S_{iz} = S \sin(2\pi\boldsymbol{\tau}\cdot\boldsymbol{r}_i + \varphi_0^i)$]. In each case, the magnetic intensity for $\boldsymbol{K} = \boldsymbol{G} \pm \boldsymbol{\tau}$ is proportional to:

$$A(\boldsymbol{K})\left|\sum_{i=5,6,11,12} \mu \exp i\left(2\pi\boldsymbol{G}\cdot\boldsymbol{r}_i + \varphi_0^i\right)\right|^2$$

with $\mu = S_{\perp} f(\boldsymbol{K})$ [$f(\boldsymbol{K})$ is the $Mn^{3+}$ magnetic form factor].

$A(\boldsymbol{K}) = 1 + \cos^2(\boldsymbol{K}, \boldsymbol{b})/4$ for a helimagnetic structure with $\boldsymbol{b}$-axis, and $A(\boldsymbol{K}) = \frac{1}{4}\sin^2(\boldsymbol{K}, \boldsymbol{c})$ for a sinusoidal modulation in the $\boldsymbol{c}$ direction.

The selection rules ($h + k + l$ even, $h$ odd) yield there $\varphi_0^{i+6} = \varphi_0^i$ ($i = 5,6$) and $\varphi_0^5 - \varphi_0^6 = \pi$, as obtained by Fricou [8] in the helimagnetic case.

The results of the profile analysis of the neutron diagram ($Mn_3O_4$, $T = 37$ K) are shown in fig. 4(a) (helimagnetic) and (b) (sinusoidal). The discrepancies in the $hkl^{\pm}$ intensities for the helimagnetic structure are evident. The reliability factors are respectively equal to:

$$R = 5.5\ (R_N = 2.8 \text{ and } R_M = 10.4) \qquad \text{(a)}$$

and

$$R = 2.55\ (R_N = 1.7 \text{ and } R_M = 4.2) \qquad \text{(b)}$$

In the later case (sinusoidal incommensurate magnetic structure) the subsequent values have been obtained for the $Mn^{2+}$ and $Mn^{3+}$ magnetic moments:

$T_y = -3.85\ (7)\mu_B$

$R_y = 1.11\ (8)\mu_B$

$R_z = 2.47\ (6)\mu_B$

$S_y = 1.05\ (10)\mu_B$

and $S_{\perp} = 1.97\ (20)\mu_B$.

All these results ($T_y$, $R_y$, $R_z$, $S_y$ and $S_{\perp}/\sqrt{2}$) are reported in fig. 3 ($T > T_t$).

### 4.2. Thermal variation of the $Mn_3O_4$ commensurate and incommensurate magnetic structures (33 K < T < 43 K)

The thermal variation of one of the $hkl^{\pm}$ magnetic Bragg peaks of fig. 4, $110^+$, is shown in fig. 5. A shift in position is observed between $T_t = 33$ and 33.4 K, without any discontinuity in intensity. Below $T_t$, $110^+$ becomes 130, when indexed in the orthorhombic $a$, $2a$, $c$ magnetic unit cell.

From the thermal variation of the angular position of $110^+/130$, the evolution of the propagation vector $\boldsymbol{\tau} \parallel \boldsymbol{b}^*$ for the $S_z$ magnetic component is obtained. The results are reported in fig. 6: $\tau$ as a function of $T$. They are in good agreement with the results of Jensen and Nielsen [7]: $q$ as a function of $T$, with $\tau = \frac{1}{2}q$.

Let us notice that the sinusoidal solution:

$$S_{i,z} = S_{\perp} \sin\left(2\pi\boldsymbol{\tau}\cdot\boldsymbol{r}_i + \varphi_0^i\right)$$

yields continuous magnetic intensities for the $\boldsymbol{K} = \boldsymbol{G} \pm \boldsymbol{\tau}$ Bragg peaks. Above $T_t$, these intensities are

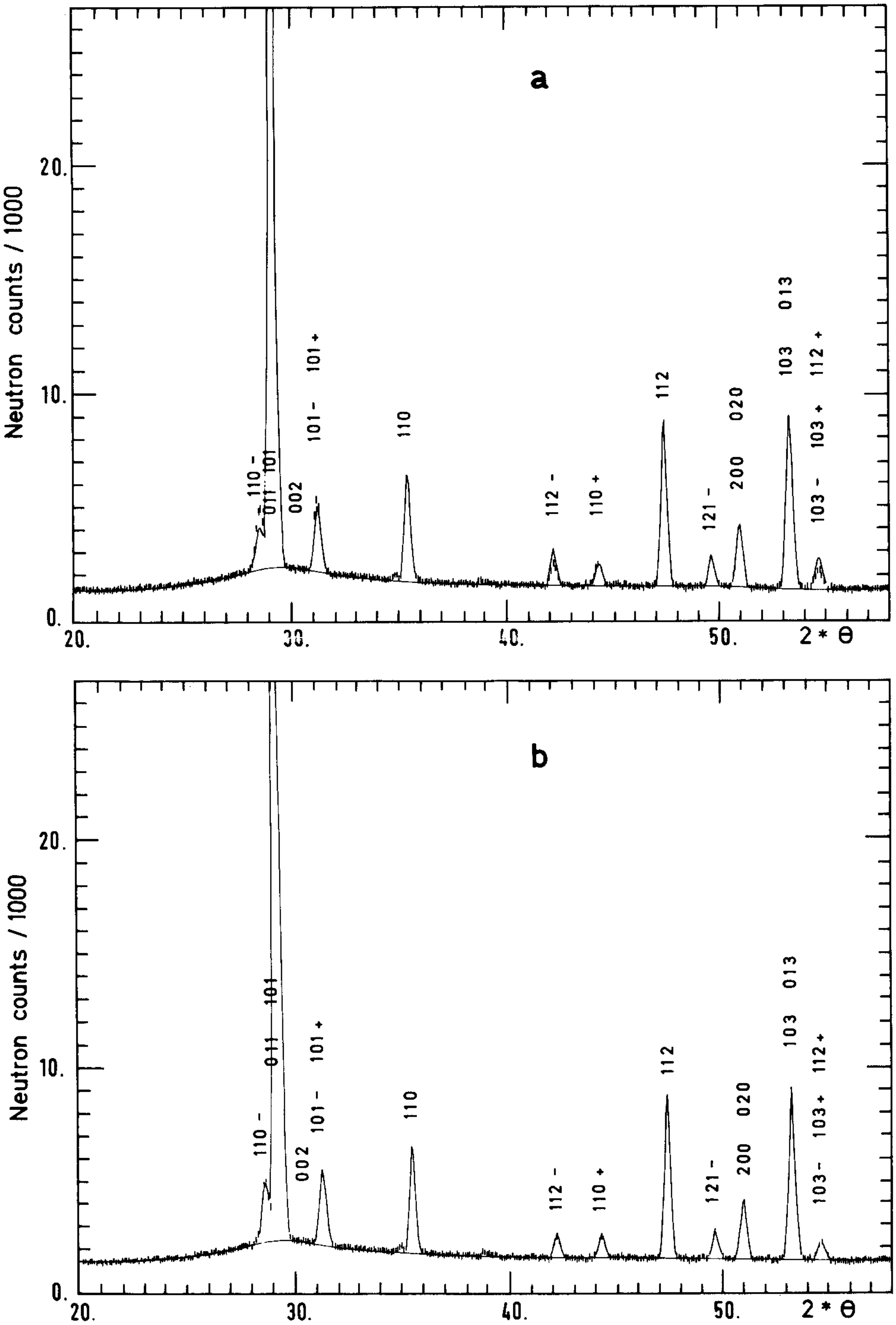


Fig. 4. $Mn_3O_4$ neutron diffraction data at $T = 37$ K ($T > T_t$). Experimental neutron counts with their accuracies are represented by vertical lines. The calculated profile (Rietveld analysis) is represented by a continuous line, corresponding for the incommensurate part of the magnetic structure (propagation vector $\tau \parallel b^*$) either to a helimagnetic structure ($S_x$ and $S_z$ components: fig. 4a) or to a sinusoidal modulation ($S_z$ component: fig. 4b).

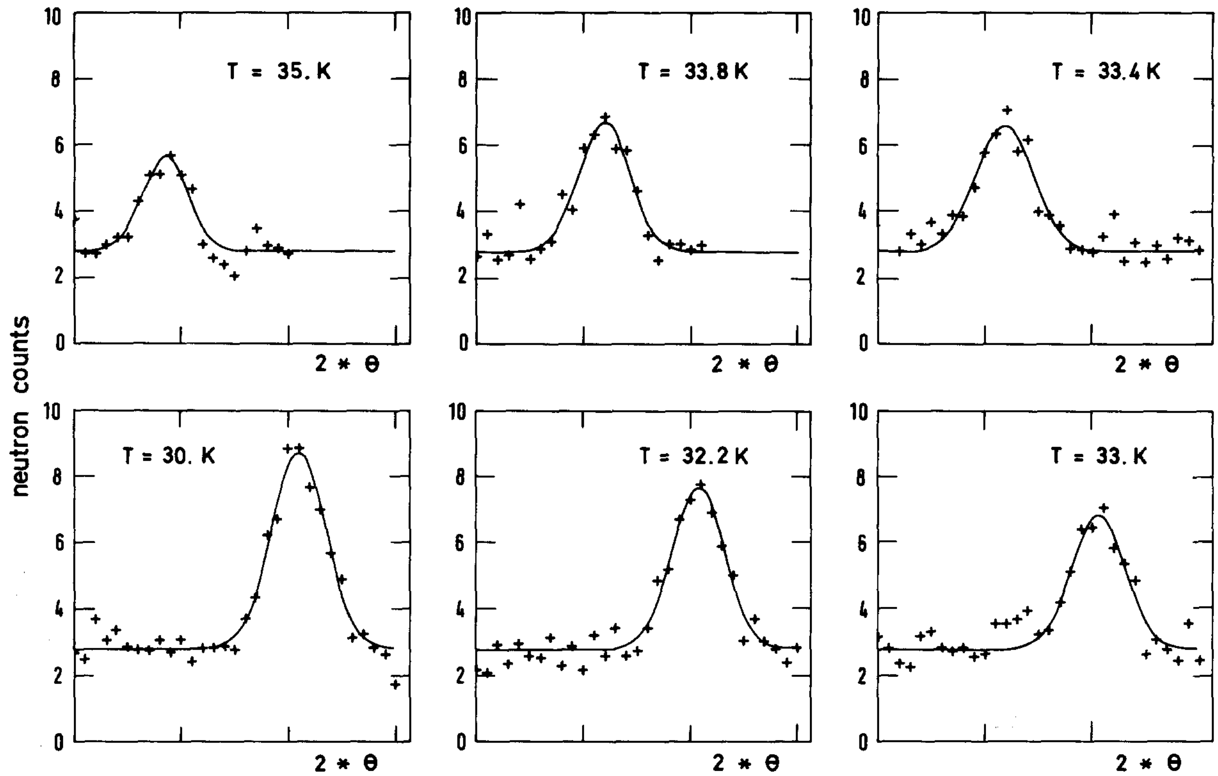


Fig. 5. Thermal variation of the 130 ($T \leq T_t$: $a, 2a, c$ magnetic cell) or $110^+$ ($T_t < T < T_C$) magnetic Bragg peak of $Mn_3O_4$. Neutron counts (arbitrary units) have been obtained for $2\theta$ varying from 43° to 46° ($\lambda = 2.46$ Å), the continuous lines in the diagrams are the calculated profiles (Gaussian form). A shift in the angular position of the peak is observed at $T_t = 33$ K, without any discontinuity in the intensity.

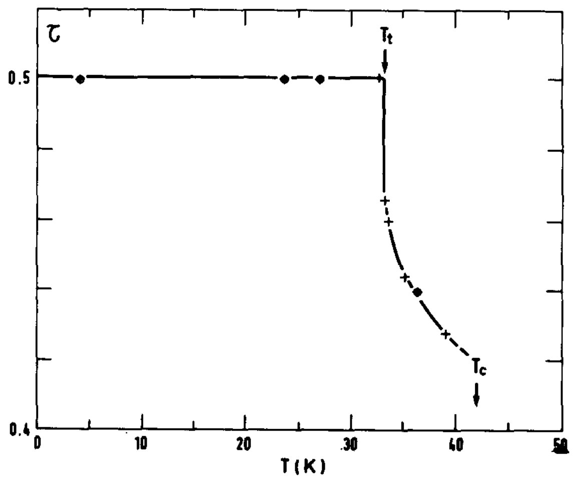


Fig. 6. Thermal variation of the propagation vector $\boldsymbol{\tau} \parallel \boldsymbol{b}^*$ for the magnetic structure of $Mn_3O_4$.

proportional to:

$$\tfrac{1}{4}\sin^2(\boldsymbol{K}, \boldsymbol{c})\left|\sum_{i=5,6,11,12} S_\perp \exp i\left(2\pi \boldsymbol{G}\cdot\boldsymbol{r}_i + \varphi_0^i\right)\right|^2$$

$$= \tfrac{1}{4}\sin^2(\boldsymbol{K}, \boldsymbol{c})\,(4S_\perp)^2$$

for $h + k + l = 2n$ and $h = 2n + 1$.

This result is independent of the value of $\varphi_0^5$. Below $T_t$, they are proportional (with the same proportionality factor) to:

$$2\sin^2(\boldsymbol{K}, \boldsymbol{S}_5 - \boldsymbol{S}_6)\|\boldsymbol{S}_5 - \boldsymbol{S}_6\|^2$$

$= 2\sin^2(\boldsymbol{K}, \boldsymbol{c})\,(2\,S_z)^2$ with $\boldsymbol{S}_5$ and $\boldsymbol{S}_6$ arranged as in fig. 1 ($Mn_3O_4$ commensurate magnetic structure).

From the comparison of these two quantities,

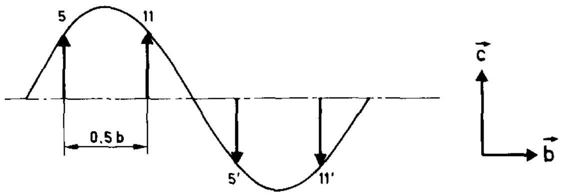


Fig. 7. Description of the $Mn_3O_4$ magnetic supers below $T_t$ as a sinusoidal modulation, with $\boldsymbol{\tau} = \frac{1}{2}\boldsymbol{b}^*$ and $\varphi_0^5 = \pi/4$.

the relation $S_z = S_\perp(\sqrt{2}/2)$ is deduced at $T_t$. Continuous curves (fig. 3) are then obtained between the low ($T < T_t$) and high ($T_t < T < T_C$) temperature values for $Mn^{2+}$ and $Mn^{3+}$ magnetic moments.

The sinusoidal solution: $S_{i,z} = S_\perp \sin(2\pi\, \boldsymbol{\tau} \cdot \boldsymbol{r}_i + \varphi_0^i)$ is shown in fig. 7, with $\boldsymbol{\tau} = \frac{1}{2}\boldsymbol{b}^*$ and $\varphi_0^5 = \pi/4$, as deduced from $S_{5,z} = S_{11,z}$. When compared with the $a$, $2a$, $c$ commensurate $S_{i,z}$ arrangement depicted in fig. 2(i), the continuity of the magnetic structure at $T_t$ is evident. (This continuity is also suggested by specific heat measurements [8,9].) The magnetic transition at $T_t$ (commensurate–incommensurate) consists there in a lock-in of the propagation vector $\boldsymbol{\tau} \| \boldsymbol{b}^*$ to the commensurate value $\frac{1}{2}\boldsymbol{b}^*$. This phenomenon has already been observed in many cases of commensurate–incommensurate magnetic phase transitions, and is due to the growing influence of the anisotropy as the temperature of the sample is lowered.

When studying the magnetic structure of $Mn_3O_4$, we also obtained neutron diffraction data at $T = 40$ K. The results of the profile refinement are given in fig. 3: a non-zero value is obtained for $R_z$, leading to a non-collinear magnetic structure, in disagreement with a previous study [5].

## Acknowledgements

The authors would like to thank M. Perrin (CEN-Saclay) for the preparation of the $Mn_3O_4$ sample. They would also like to thank E. Roudaut and M. Pailly (CEN-Grenoble), Y. Allain (CEN-Saclay) for their cooperation in the neutron diffraction experiments. They are grateful to P. Mériel (CEN-Saclay) for helpful discussions.

## References

[1] B. Boucher, R. Buhl and M. Perrin, J. Phys. Chem. Solids 32 (1971) 2429.
[2] J.B. Goodenough and A.L. Loeb, Phys. Rev. 98 (1954) 391.
[3] K. Dwight and N. Menyuk, Phys. Rev. 119 (1960) 1470.
[4] O.V. Nielsen, J. Phys. Coll. 32, Suppl. C1 (1971) 51.
[5] G. Srinivasan and M.S. Sheera, Phys. Rev. B28 (1983) 1.
[6] F.K. Lotgering, Philips Res. Rep. 11 (1956) 190.
[7] G.B. Jensen and O.V. Nielsen, J. Phys. C7 (1974) 409.
[8] B. Fricou, Thesis, Université Paris VI (1977).
[9] C. Pommier, K. Chhor and B. Chardon, J. Chem Thermodyn. (submitted).
[10] B. Chardon, Thèse Docteur Ingénieur, Université Paris VI (1984).
[11] E. Roudaut, in: Position Sensitive Detection of Thermal Neutrons, eds. P. Convert and J.B. Forsyth (Academic Press, New York, 1983) p. 294.
[12] H.M. Rietveld, J. Appl. Cryst. 2 (1969) 65.